EXPERIMENTAL ASSESSMENT OF LOCAL WALL THINNING OF A PROCESS PIPING ELBOW

Cristian - Mihai PETRE[1], Alin DINIȚĂ[2]*, Ibrahim Naim RAMADAN[3]

Fatigue tests were performed using test bodies made from process piping elbows without and with local wall thinning. Local wall thinning was machined to simulate metal loss – located inside the extrados of the elbow. The elbow specimens were subjected to cyclic in-plane bending under displacement control without and with internal pressure. Strains were recorded by strain gauges and principal and equivalent stresses were calculated. A modelling of test elbow specimen by finite element method was done to evaluate the loading previous to testing.

Keywords: steel pipe, elbow, cycle fatigue, local wall thinning, finite element analysis (FEA), strain analysis.

1. Introduction and review

Elbows are critical elements of pipes, because they are subjected to erosion-corrosion due to fluid flow changing of direction and also has a higher stress concentration in comparison with line eÎlements of pipes. [1].

Methods for evaluating fatigue strength are more complex than for static mechanical tests, time consuming, use complex equipment and interpretation of test results is more difficult [2],[3],[4]. This is due to the difficulty to detect the starting moment of deterioration and the results of fatigue tests show a large dispersion compared to the results of other tests. Fatigue strength is influenced by constructive and technological factors [3][4]: quality and homogeneity of the material or the presence of material defects and the quality of the component surface, the operating conditions of the component – overloads, the degree of asymmetry of the stress cycles, or the influence of the environment due to corrosion.

Takahashi et al. have performed experimental tests with the scope of developing a methodology for assessing the integrity of piping components with local wall thinning [5][6][7]. Tests were carried out for: straight pipes [6][7], elbows [5][6], tees and orifices [6][7], and analytical models for evaluating the

[1] Ph.D. Stud. Eng., Petroleum – Gas University of Ploiesti, Romania, e-mail: cristianmihai_petre@yahoo.com
[2] Assoc. prof. dr. eng., Dept. Mechanical Engineering, Petroleum – Gas University of Ploiesti, Romania, e-mail: adinita@upg-ploiesti.ro
[3] Lect., dr. eng., Dept. Mechanical Engineering, Petroleum – Gas University of Ploiesti, Romania, e-mail: ing_ramadan@yahoo.com

integrity of the piping systems were proposed; most of studies follow a monotonic rather than cyclic loading.

It is important to establish a safety margin of old and degraded piping against occasional loading since there are components that are more sensitive to erosion/corrosion, this beeing exacerbated at elbows [5],[6],[7]. For this static and fatigue studies were carried out. In his researches, Takahashi et al. [5],[6],[7], and Vishnuvardhan et al. [8],[9], follows an experimental procedure and finite element analyses (FEA) carried out to accurately simulate fracture behavior and to investigate the effects of local wall thinning on the fracture behaviors of pipe components – local wall thinning was machined on the inside of piping components to simulate metal loss due to corrosion. Loading of the area with local wall thinning leaded to either tensile or compressive stress; also the relative opening / closing movement between the two ends is an important factor in controlling fatigue life. Based on the thickness ratio, and stress at the local wall thinning failure type was classified into ovalization, local buckling and crack initiation.

Other experiments were performed by Vishnuvardhan et al. [8], Hanes et al. [10] and Dahlberg et al. [11], for fatigue on a non-welded water pressurized piping component made of austenitic stainless steel for high and low cyclic fatigue. The components were loaded at a variable amplitude bending deformation to compare with the results obtained for a similar piping component with a hoop butt weld in order to determine an experimental fatigue strength reduction factor and also to investigate the margins of the American Society of Mechanical Engineers (ASME) design curve for austenitic stainless steel.

Research by Harun et al. [1], adopted the methodology for integrity of high-strength carbon steel pipe elbows weakened by local pipe wall thinning with focus on low cyclic fatigue behavior of damaged elbows, in relation to strength and integrity of piping of nuclear power plants (NPP) subjected to severe occasional loading and extends it to elbows from copper-nickel. Tested elbows with local wall thinning at different locations demonstrate a significant safety margin; the increase of fatigue life with the increase of the applied inner pressure, can be explained by the fact that the applied bending load is relaxed by the inner pressure.

The aim of this article is to determine the mechanical stresses considering experimental and finite element analyses for a hollow element welding fitting (a 90° elbow) subjected to cyclic stresses and stresses resulting of composed loading from symmetric cyclic in plane bending and simultaneous static internal pressure. The results of the tests are presented (internal pressure and cyclic loading) for the aforementioned element which has an anomaly (local wall thinning) inside it.

2. Materials and methods

Several stages of experiments are followed in tests of two sample bodies: first stage for a specimen without defect and a second stage for a similar specimen having an inside simulated defect.

A. Sample elbow without defect

Experimental sample bodies were built for cyclic testing, as shown in Figure 1, assembled from: an elbow welded with two pipe spools of the same steel grade, outside diameter and wall thickness ended in two plugs with clamping lugs and fixture elements for the Universal Testing Machine (UTM). The mechanical properties and chemical composition of P265GH steel for elbows are listed in Tables 1 and 2, according to [12].

Table 1

Mechanical properties of steel P265GH

R_m - Tensile strength [MPa]	410-530		
R_{eH} - Minimum yield strength [MPa]	265		
KV - Impact energy [J]	27 (-20°)	27 (0°)	40 (+20°)
KV - Impact energy [J] longitudinal,	28 (-10°)	40 (0°)	47 (+20°)
A – Minimum elongation at fracture [%]	22-23		
A – Minimum elongation at fracture [%] transverse	21		

Table 2

Chemical composition of P265 GH steel, maximum %

C	Si	Mn	Ni	P	S	Cr	Mo	V	N	Nb	Ti	Al	Cu
0.2	0.4	0.8 - 1.4	0.3	0.025	0.015	0.3	0.08	0.02	0.012	0.02	0.03	0.02	0.3

Parts of the specimen are shown in Figure 1 (a) and (b) and were used for recording mechanical strains during cyclic loading tests: (1) an elbow (EN 10253 – 3, [13]) of 90°, with Ø 88.9×3.2 mm and a bending radius of 114.3 mm from P265 GH steel grade; two pipe spools of Ø 88.9×200×3.2 mm (2); hinge subassemblies (3) from two weldable plug with clamping lug (Ø 90×110 mm); two fasteners fork-type for the clamping dies of the UTM (4); bolts for mounting (5); HBM MGCplus system for strain data acquisition (6); Catman Easy application for data acquisition (7); UTM Walter + Bai LF300, 30kN (8). Strain gauges (SG) for axial and hoop measuring directions were installed and measurements were performed at four points in the plane of symmetry of the elbow as per Table 3, and depicted in Figure 2.

Table 3

Placement of strain gauges on elbow and measurement direction

Measurement Direction, (Fig. 3)	SG measurement left side and right side	SG measurement extrados and intrados
Axial	1 and 5	3 and 7
Hoop	2 and 6	4 and 8

In the first stage of experiments the specimens without defects were subjected to three static loading steps at certain forces and displacements and then in three sequences of cyclic in plane bending under displacement control in accordance to static loadings displacements, without internal pressure. For this stage, details of the loading sequences at a frequency, *f* of 5Hz, are shown in Table 4.

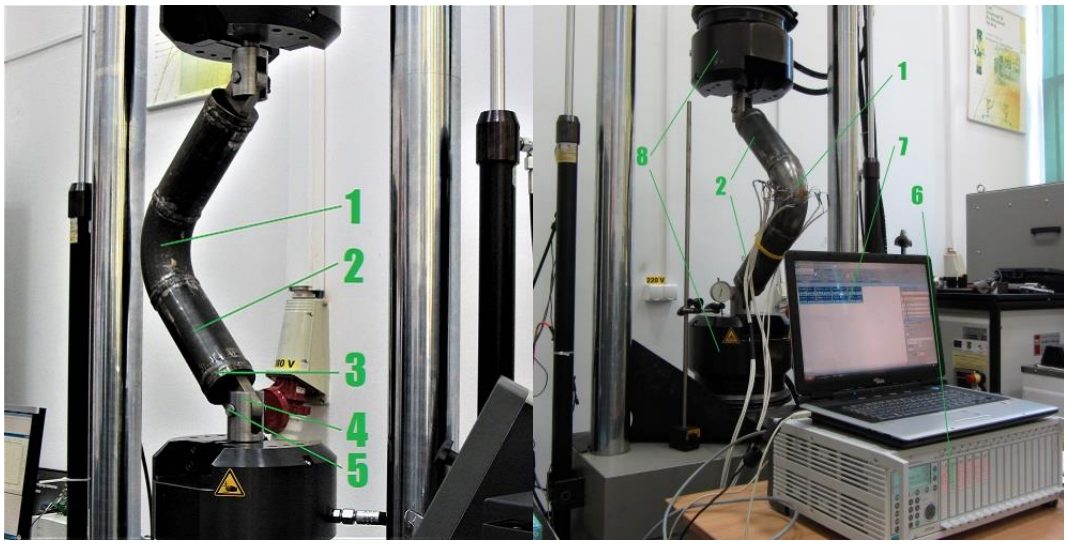

(a) Experimental specimen (b) Recording strains at cyclic loading with SG

Fig. 1 Experimental specimen for cyclic loading (fatigue) tests

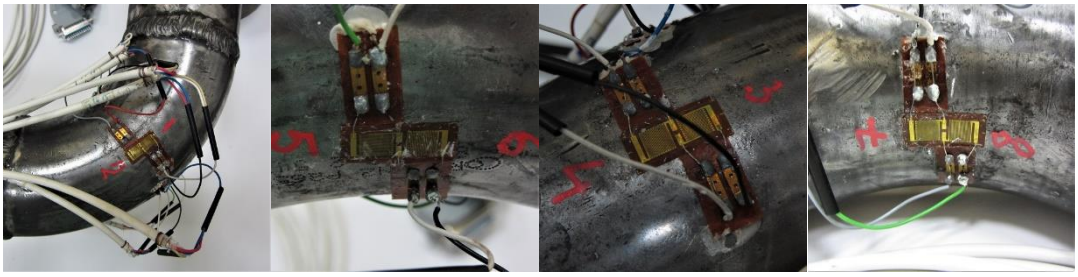

(a) (b) (c) (d)

Fig. 2 Strain gauges placed on the elbow: left side SG 1 and 2 (a), right side SG 5 and 6 (b), at extrados SG 3 and 4 (c), intrados SG 7 and 8 (d)

Table 4

1st stage experiments cyclic in plane bending loading on the specimen without defects

Static Loading			Cyclic loading with displacement control		
Applied load, [kN]	Tensile, [mm]	Compression, [mm]	Loading sequence range, [mm]	Time of loading sequence, [s]	Number of cycles per sequence
1.0	0.42	-0.40	- 0.5 ... + 0.5	19 837	99185
2.0	0.85	-0.83	- 0.7 ... + 0.7	19 837	99185
3.0	1.27	-1.28	- 0.9 ... + 0.9	16 592	82960

B. Sample elbow with defect

For the second elbow sample in order to simulate a defect with an irregular geometric pattern on the inner elbow surface, prior to assembly, the inside surface was processed by grinding with a straight grinder resulting in the surface shown in Figure 3 (a). To facilitate the measurement of the wall thickness of the elbow in the area affected by notches, a grid was drawn on the outer surface of the elbow with 85 measuring points equidistantly in hoop and axial direction – at 10 mm distance, as shown in Figure 3 (b) and (c). Measured wall thicknesses with ultrasonic thickness gauge are in Table 5.

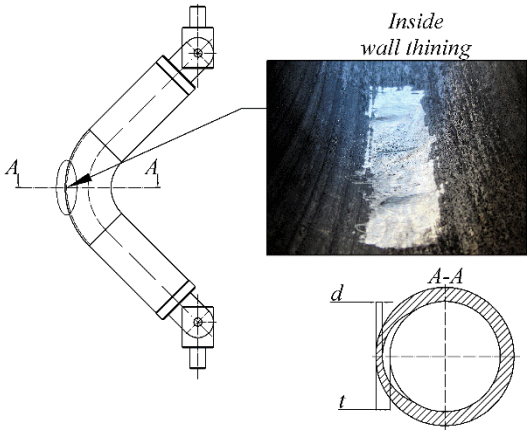

(a) Image of the inside elbow prior to welding; the inner surface of the elbow was splintered with a small straight grinder to simulate a local wall thinning defect

(c) image of the outside grid

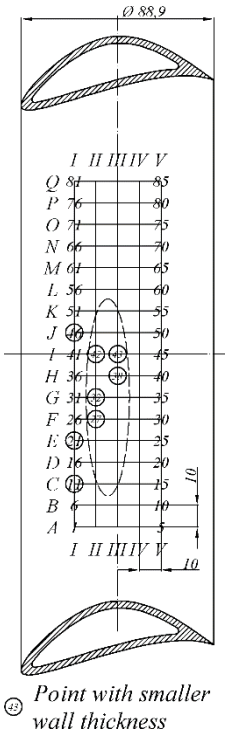

(b) Detail drawing to identification of the points – measurement grid on the outer surface of the elbow corresponding to hidden inside wall thinning area (median plane through the elbow corresponds to the profile line III)

Fig. 3 Simulation of an inside wall thinning type defect with an irregular geometric pattern

To characterize metal loss in the wall thickness direction the ratio between wall thickness in flaw point (d) to the nominal wall thickness (t) is defined (d/t) – eroded ratio. This ratio, for the smallest wall thickness (grid point 32) has a value of $d/t = 2.31/3.2 = 0.72$ (a local wall thinning of 28 %).

In the second stage of experiments the specimen with inside wall thinning was subjected to sequences of loading with internal pressure combined with cyclic in plane bending under displacement control, as per loading sequences shown in Table 5, at a frequency, *f* of 5Hz.

Table 5

2nd stage of experiments cyclic combined loading on the specimen with defects

Internal pressure steps, [MPa]	Displacement range Δ, [mm]	Number of cycles per sequence
0	± 0.25	1344
	± 0.42	939
	± 0.50	499
	± 0.75	263
	± 1.00	507
2	± 0.25	2224
	± 0.50	118
	± 0.75	595
	± 1.00	1977
4	± 0.25	328
	± 0.50	189
	± 0.75	2459
	± 1.00	317
6	± 0.25	301

C. Finite Element Analysis

For the assessments of the applied displacement and loading a linear elastic finite element analysis (FEA) in Ansys APDL was carried out. The model has 7666 SHELL93 elements and 20646 nodes; different loadings were considered (see Table 1) along the axis of the lifting lug.

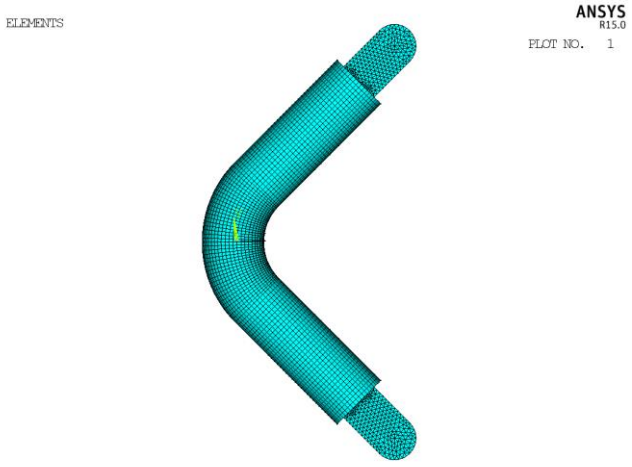

Fig. 4 FEA model for the specimen.

3. Results and discusions

Influence of the defect was considered by a calculation of stresses (as per EN 13480 – 3) due to internal pressure for each measured wall thickness in the grid points; input data for measured wall thicknesses are given in Table 7.
From the measuring grid considering points that lay on the same longitudinal reference grid line, longitudinal wall thickness and effective stress due to internal pressure profiles were plotted. For this, calculation of effective stress values was done with relation (1) from [14], and resulting longitudinal wall thickness and effective stress profiles are plotted in Figure 5 (a) and (b).

$$\sigma = \frac{p_C \cdot (D_o - e)}{2 \cdot e \cdot z} \tag{1}$$

Where: e – measured pipe wall thickness;
Results of calculation to internal pressure for input data given in Tables 6 and 7 for each measured wall thickness in the grid points are presented in Table 8.

Table 6

Input data used for calculation of stresses in grid points affected by local wall thinning

Description	Value	Description or designation	Value
Material	P265GH	Thinning allowance for possible thinning during manufacturing process, c_2, [mm]	0
Nominal Diameter, DN	80		
Outside Diameter, D_o [mm]	88.9		
Operating temperature, t, [ºC]	20	Minimum required thickness with allowances and tolerances, e_r, [mm]	3.18
Calculation temperature, t_c, [ºC]	20		
Minimum specified value of tensile strength at room temperature, R_m, [MPa]	410	Maximum allowable pressure, PS, [MPa]	7
		Minimum specified value of upper yield strength at room temperature, R_{eh}, [MPa]	265
Minimum specified value of 0.2 % proof strength at calculation temperature t when this temperature is greater than the room temperature, $R_{p0,2}^t$, [MPa]	265	Minimum specified value of upper yield strength at calculation temperature when this temperature is greater than the room temperature, R_{eH}^t, [MPa]	265
Allowable design stress, σ, [MPa]	170.833		
Calculation pressure, p_c, [MPa]	7		
Weld joint coefficient, z	1	95 % of the minimum specified value of upper yield strength at calculation temperature when this temperature is greater than the room temperature, $0.95 \cdot R_{eH}^t$, [MPa]	251.750
Corrosion or erosion allowance, c_0, [mm]	1		
Ordered thickness, e_{ord}, [mm]	3.2		
Absolute value of the negative tolerance taken from the material standard, c_1, [mm]	0.4	Test stress at test temperature, f_{test}, [MPa]	170.833

As a result, in point 32 of the grid was found a maximum value for effective stresses of 131.2 MPa.

Table 7

Initial wall thicknesses measured with ultrasonic thickness gauge

No.	**1**	**2**	**3**	**4**	**5**	**6**	**7**	**8**	**9**	**10**	**11**	**12**
e	2.68	2.91	2.92	2.88	2.99	2.7	2.85	3.02	3.02	3.12	2.77	2.96
No.	**13**	**14**	**15**	**16**	**17**	**18**	**19**	**20**	**21**	**22**	**23**	**24**
e	2.94	2.93	3	2.78	2.92	2.96	2.92	3.07	2.75	2.95	2.88	2.91
No.	**25**	**26**	**27**	**28**	**29**	**30**	**31**	**32**	**33**	**34**	**35**	**36**
e	3.05	2.78	2.65	2.89	2.86	3.02	2.92	2.31	2.86	3.03	3.02	2.77
No.	**37**	**38**	**39**	**40**	**41**	**42**	**43**	**44**	**45**	**46**	**47**	**48**
e	2.78	2.63	2.9	2.99	2.83	2.38	2.76	3.01	3.09	2.75	3.05	2.88
No.	**49**	**50**	**51**	**52**	**53**	**54**	**55**	**56**	**57**	**58**	**59**	**60**
e	3.02	3.08	3.09	3.11	3.18	2.94	3.07	3	3.06	2.98	3	3.21
No.	**61**	**62**	**63**	**64**	**65**	**66**	**67**	**68**	**69**	**70**	**71**	**72**
e	3.02	3.03	3.07	3.05	3.2	3.08	3.18	3.21	2.89	3.02	2.87	3.25
No.	**73**	**74**	**75**	**76**	**77**	**78**	**79**	**80**	**81**	**82**	**83**	**84**
e	3.05	3.02	3.06	2.88	3.03	3.01	2.91	3	3.05	2.77	3	3.07
No.	**85**	**No. = Wall thickness measurement point on grid elbow surface**										
e	2.95	***e* = Measured pipe wall thickness, [mm]**										

Table 8

Effective stresses result for corresponding grid points affected by local wall thinning

No.	**1**	**2**	**3**	**4**	**5**	**6**	**7**	**8**	**9**	**10**	**11**	**12**
Strs.	112.6	103.4	103.1	104.5	100.6	111.7	105.7	99.5	99.5	96.2	108.8	101.6
No.	**13**	**14**	**15**	**16**	**17**	**18**	**19**	**20**	**21**	**22**	**23**	**24**
Strs.	102.3	102.7	100.2	108.4	103.1	101.6	103.1	97.9	109.6	102.0	104.5	103.4
No.	**25**	**26**	**27**	**28**	**29**	**30**	**31**	**32**	**33**	**34**	**35**	**36**
Strs.	98.5	108.4	113.9	104.2	105.3	99.5	103.1	**131.2**	105.3	99.2	99.5	108.8
No.	**37**	**38**	**39**	**40**	**41**	**42**	**43**	**44**	**45**	**46**	**47**	**48**
Strs.	108.4	114.8	103.8	100.6	106.4	127.2	109.2	99.9	97.2	109.6	98.5	104.5
No.	**49**	**50**	**51**	**52**	**53**	**54**	**55**	**56**	**57**	**58**	**59**	**60**
Strs.	99.5	97.5	97.2	96.5	94.3	102.3	97.9	100.2	98.2	100.9	100.2	93.4
No.	**61**	**62**	**63**	**64**	**65**	**66**	**67**	**68**	**69**	**70**	**71**	**72**
Strs.	99.5	99.2	97.9	98.5	93.7	97.5	94.3	93.4	104.2	99.5	104.9	92.2
No.	**73**	**74**	**75**	**76**	**77**	**78**	**79**	**80**	**81**	**82**	**83**	**84**
Strs.	98.5	99.5	98.2	104.5	99.2	99.9	103.4	100.2	98.5	108.8	100.2	97.9
No.	**85**	**No. = Measurement point on elbow surface**										
Strs.	102.0	**Strs. = Effective stress corresponding to No., [MPa]**										

Through experimental stress analysis by strain gauge strains are measured, used to calculate the values of the principal stresses – for a specific point in a structural element. If the stresses do not exceed the yield limit of the material the following stresses are computed by Hooke's generalized law for plane stresses: the first principal stress σ_θ acting in the tangential direction of the circumference (2) and the second principal stress σ_a acting in the axial direction (3).

$$\sigma_\theta = \frac{E}{1-\mu^2}\cdot\left(\varepsilon_\theta + \mu\cdot\varepsilon_a\right) \tag{2}$$

$$\sigma_a = \frac{E}{1-\mu^2}\cdot\left(\varepsilon_a + \mu\cdot\varepsilon_\theta\right) \tag{3}$$

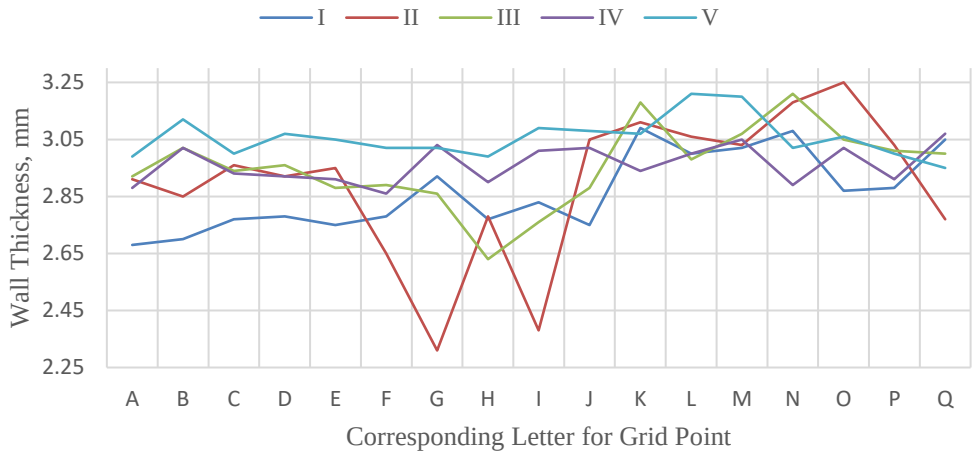

(a) Longitudinal wall thickness profile

Grid line	Corresponding No. and Letter for Grid Point (Figure 4)																
	A	**B**	**C**	**D**	**E**	**F**	**G**	**H**	**I**	**J**	**K**	**L**	**M**	**N**	**O**	**P**	**Q**
I	1	6	11	16	21	26	31	36	41	46	51	56	61	66	71	76	81
II	2	7	12	17	22	27	32	37	42	47	52	57	62	67	72	77	82
III	3	8	13	18	23	28	33	38	43	48	53	58	63	68	73	78	83
IV	4	9	14	19	24	29	34	39	44	49	54	59	64	69	74	79	84
V	5	10	15	20	25	30	35	40	45	50	55	60	65	70	75	80	85

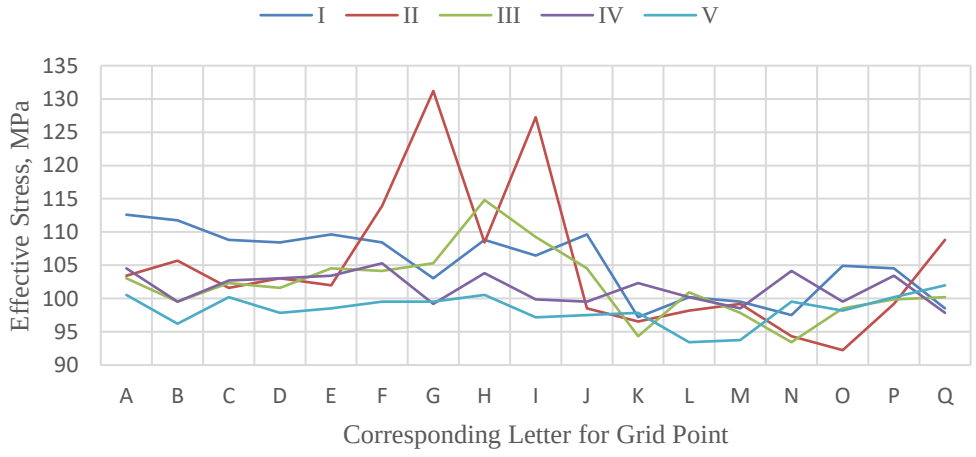

(b) Longitudinal effective stress profile, for PS (7MPa) calculated with (1)

Fig. 5 Profile lines measured and calculated for grid points

With the experimental data recorded – strains for each SG and by means of formulae (2) and (3), with the value of the Poisson's coefficient μ, and E, Young modulus (μ = 0.3 and E = $2.1 \cdot 10^5$ MPa), mechanical stresses for axial σ_a and hoop σ_θ and von Mises criterion equivalent stresses were calculated and presented in Table 9 and 10.

Table 9

Experimental stresses as per axial σ_a and hoop σ_θ directions computed from the SG strains

Applied force, [kN]	Left crown		Extrados		Right crown		Intrados	
	σ_a SG 1	σ_θ SG 2	σ_a SG 3	σ_θ SG 4	σ_a SG 5	σ_θ SG 6	σ_a SG 7	σ_θ SG 8
Tensile, [MPa]								
1	-35.33	-23.94	-35.09	-30.80	4.61	10.21	15.28	18.89
2	-71.00	-48.09	-69.98	-61.02	9.27	20.53	30.54	37.92
3	-106.07	-70.62	-102.86	-89.79	13.88	30.92	45.79	56.93
Compression, [MPa]								
1	36.86	26.67	34.95	29.96	-4.50	-10.58	-15.62	-19.50
2	72.92	52.78	71.01	59.97	-8.98	-20.64	-30.82	-38.35
3	110.16	79.22	108.64	91.00	-13.60	-31.06	-46.56	-57.83

From the static loads a graph of the dependence between the applied force and displacement was drawn in Figure 6, proving that loading remained symmetric. Based on the values for principal stresses for static loading the equivalent stresses were calculated with relation (4). The graph of the dependence between the values of the von Mises equivalent stresses and displacement was plotted in Figure 7, stresses remaining in the linear elastic domain.

$$\sigma_{Mis} = \sqrt{\sigma_a^2 + \sigma_\theta^2 - \sigma_a \sigma_\theta} \tag{4}$$

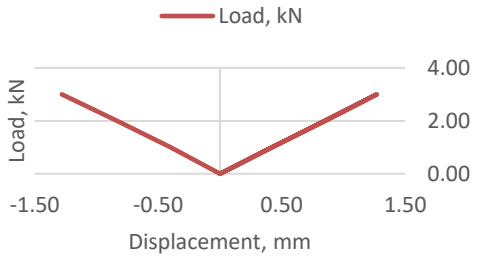

Fig. 6 Graph of dependence between applied load force and displacement

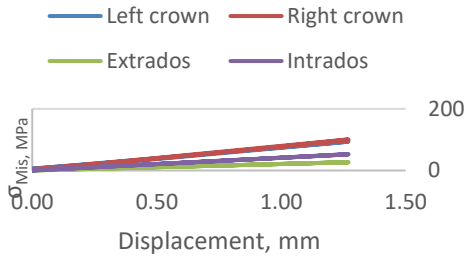

Fig. 7 Dependence between equivalent von Mises stresses (σMis, MPa) and displacement

Resulting equivalent stress maps for 1 kN applied load, from crown to extrados and to intrados and the inner surface of the elbow are shown in Figure 8; similar shape and location for stress maps are found in [1],[5].

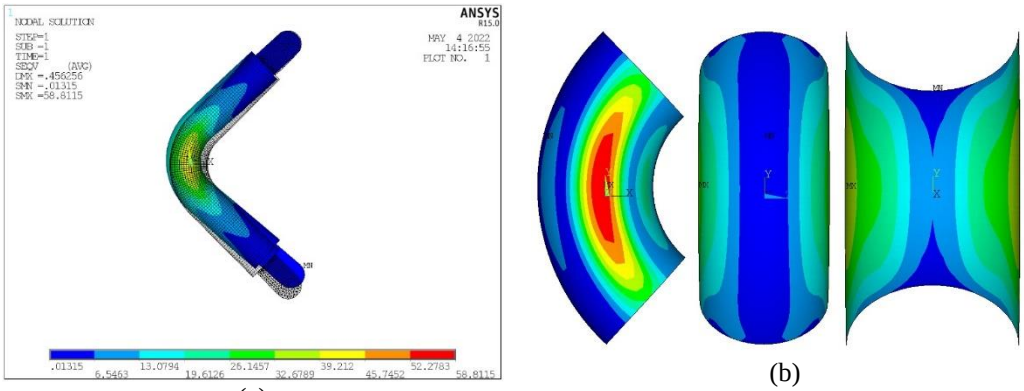

(a) (b)

Fig. 8 FEA stresses maps for 1kN applied load: (a) von Mises criterion map, (b) stress map of inner surface.

For the combined cyclic loading in plane bending and internal pressure strains were acquired and recorded for each SG.

Table 10

von Mises criterion σ_{Mis} and FEA equivalent stresses at the measurement points

Applied force, [kN]	Left crown			
	Tensile, [MPa]	FEA, [MPa]	Compression, [MPa]	FEA, [MPa]
1	31.23	33.79	32.97	35.92
2	62.77	68.73	65.22	71.53
3	93.53	102.69	98.41	107.66
Applied force, [kN]	Right crown			
	Tensile, [MPa]	FEA, [MPa]	Compression, [MPa]	FEA, [MPa]
1	33.15	36.08	32.74	35.55
2	65.96	72.04	66.18	72.20
3	96.99	106.61	100.98	110.77
Applied force, [kN]	Extrados			
	Tensile, [MPa]	FEA, [MPa]	Compression, [MPa]	FEA, [MPa]
1	8.86	9.58	9.20	9.96
2	17.80	18.69	17.92	19.56
3	26.82	29.46	26.97	29.58
Applied force, [kN]	Intrados			
	Tensile, [MPa]	FEA, [MPa]	Compression, [MPa]	FEA, [MPa]
1	17.37	18.82	17.88	19.41
2	34.82	38.17	35.20	38.62
3	52.26	57.41	53.10	58.34

Mechanical stresses (axial σ_a and hoop σ_θ), and von Mises stresses were computed for the second stage of experiments – using the relations (2) and (3)

between acquired strains and Poisson's coefficient μ, and Young modulus for principal stresses. Von Mises stresses ranges are listed in Table 11. It has been found that for stress cycles with different degrees of asymmetry the fatigue strength is different, and for stresses due to symmetrical alternating cycle, minimum fatigue strength values are obtained, [3],[4].

Table 11

Stress range (minimum ... maximum) von Mises criterion for combined loading

p, [MPa]	*Δ*, [mm]	Left, [MPa]	Extrados,[MPa]	Right, [MPa]	Intrados,[MPa]
0	±0.25	0.3 ... 2.7	0.1 ... 0.7	2.3 ... 3.7	0.1 ... 1.6
	±0.42	0.0 ... 10.7	0.0 ... 2.3	0.0 ... 9.3	0.1 ... 5.9
	±0.50	0.2 ... 10.5	0.0 ... 2.1	0.2 ... 9.2	0.0 ... 5.7
	±0.75	50.1 ... 134.2	10.9 ... 29.1	46.0 ... 122.2	28.0 ... 75.0
	±1.00	57.5 ... 148.8	12.2 ... 32.1	53.3 ... 136.6	32.2 ... 83.5
2	±0.25	0.4 ... 32.1	0.1 ... 3.1	0.0 ... 10.2	0.0 ... 12.6
	±0.50	0.0 ... 24.7	0.0 ... 5.4	0.0 ... 22.5	0.0 ... 14.6
	±0.75	0.6 ... 30.3	0.0 ... 6.8	0.2 ... 28.5	0.5 ... 22.5
	±1.00	0.5 ... 21.0	0.0 ... 3.8	0.1 ... 16.9	0.8 ... 9.4
4	±0.25	0.3 ... 21.8	0.0 ... 4.6	0.1 ... 19.8	0.1 ... 12.6
	±0.50	0.0 ... 32.9	0.0 ... 7.2	0.0 ... 30.0	0.0 ... 19.5
	±0.75	16.1 ... 69.5	3.3 ... 15.6	14.5 ... 63.4	9.0 ... 41.7
	±1.00	0.1 ... 130.6	0.0 ... 29.1	0.0 ... 118.9	0.1 ... 77.8
6	±0.25	0.1 ... 17.2	0.1 ... 3.8	0.2 ... 15.6	0.3 ... 10.8

Typical graphs of dependence between stress and strains for combined loading due to applied displacement *Δ* ± 1 mm and steps of internal pressure 0; 20 and 40 bars are plotted in Figure 7.

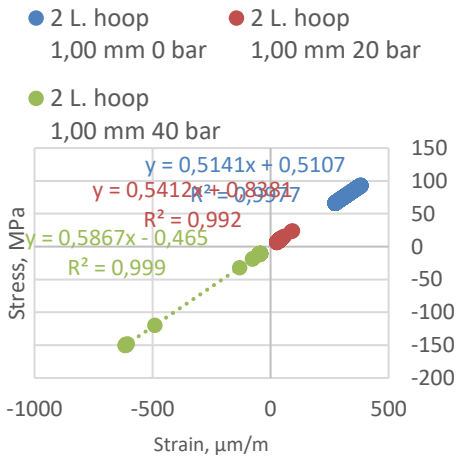

Fig. 7 Typical graph of dependence between hoop stress and strains for left side (L.) crown of elbow due to combined loading displacement and internal pressure

4. Conclusions

Fatigue behavior at room temperature of process piping elbows from P265 GH steel (Ø 88.9 × 3.2 mm and radius of 114.3 mm) with and without internal anomalies was experimentally investigated subjecting them to steady internal pressure and cyclic bending load. Experimental results, analytical calculation and FEA lead to the following conclusions:

- fatigue studies were carried out under combined internal pressure and in-plane bending. Fatigue strain was recorded in the hoop direction at the intrados, crown and at the extrados by strain gauge measurements;
- the maximum stress is found at crown (left/right) area, the intrados is at an intermediate level, while the minimum stress appears at the extrados of elbows. This behaviour is also found in elbows specimens studied in other scientific papers [1][2][5][9];
- the result obtained in [5] at extrados pipe regarding that the most strain-concentrated point occurred at the inner surface of the crown, regardless of wall thinning at the extrados, was also confirmed by present study;
- the most strain-concentrated point occurred at the inner surface of the crown specimen as highlighted in [5] for elbows without defects;
- to highlight the influence of anomalies (internal defects e.g. transverse grooves), analytical calculation of stresses (as per EN 13480 – 3) due to internal pressure for each measured wall thickness in the grid point was done;
- for load values corresponding to displacements of ±1.00 mm and 0 bar maximum values of strains and resulting stresses (main and equivalent von Mises criteria) were recorded for all strain analysis points. As the specimen is pressurized, the bending moment is reduced and the stiffness of the elbow is increased, even though the displacement is maintained at a given value – the applied bending load is relaxed by the internal pressure, a similar behaviour being found in [1][5];
- the reduction of the ovalization and local stress accumulation was found also for defectless elbows.

As it is emphasized in [1]: more work is required to clarify the explicit safety margin of elbows with defects, the influence of location and severity of wall thinning, eroded ratio, and applied pressure. Local wall thinning at extrados and intrados does not affect cyclic fatigue life of damaged elbows; in most cases, fatigue fails in the crown regions where stresses increases to maximum values.

REFERENCES

[1] *M.F. Harun, R. Mohammad, A. Kotousov*, Low cycle fatigue behavior of elbows with local wall thinning, Metals 2020, **10**, 260

[2] *Y. S. Yoo, S. H. Ahn, K. W. Nam, K. Ando, S. H. Ji, M. Ishiwata, K. Hasegawa*, Fracture Behavior of Straight Pipe and Elbow with Local Wall Thinning, Transactions, SMiRT 16, Washington, August 2001

[3] *Ș. Nădășan, B. Horovitz, A. Bernath, V. Safta,* Metal Fatigue (Romanian: Oboseala Metalelor), Editura Tehnică, București, 1962

[4] *A. Pupăzescu*, Theoretical mechanics and strength of materials, (Romanian: Mecanică teoretică și rezistența materialelor) Editura Universității Petrol-Gaze din Ploiești, Ploiești, 2007

[5] *K. Takahashi, S. Tsunoi, T. Hara, T. Ueno, A. Mikami, H. Takada, K. Ando, M. Shiratori*, Experimental study of low-cycle fatigue of pipe elbows with local wall thinning and life estimation using finite element analysis, International Journal of Pressure Vessels and Piping **87** (2010) 211 – 219

[6] *K. Takahashi, A. Kato, K. Andoa, M. Hisatsune, K. Hasegawa*, Fracture and deformation behaviors of tee pipe with local wall thinning, Nuclear Engineering and Design **237** (2007) 137–142

[7] *K. Takahashi, K. Andoa, M. Hisatsune, K. Hasegawa*, Failure behavior of carbon steel pipe with local wall thinning near orifice, Nuclear Engineering and Design **237** (2007) 335–341

[8] *S. Vishnuvardhan, G. Raghava, P. Gandhi, M. Saravanan, D. M. Pukazhendhi, S. Goyal, P. Arora, S. K. Gupta*, Fatigue ratcheting studies on TP304 LN stainless steel straight pipes, Procedia Engineering **2** (2010) 2209–2218

[9] *S. Vishnuvardhan, G. Raghava, P. Gandhi, S. Goyal, S. K. Gupta, V. Bhasin*, Ratcheting Strain Assessment in Pressurised Stainless Steel Elbows Subje cted to In-plane Bending, 6th International Conference on Creep, Fatigue and Creep-Fatigue Interaction [CF-6], Procedia Engineering **55** (2013) 666 – 670

[10] *D. Hanes, T. Svensson, A. Anderson, M. Dahlberg*, Experimental study of weld fatigue strength reduction for a stainless steel piping component, 7th International Conference on Fatigue Design, 2017, Senlis, France, 2017, Procedia Engineering **213** (2018) 383–391

[11] *M. Dahlberg, D. Hannes, T. Svensson*, Evaluation of fatigue in austenitic stainless steel pipe components, Strålsäkerhetsmyndigheten, Swedish Radiation Safety Authority, SSM 2015:38, ISSN: 2000-0456

[12] ∗ ∗ ∗ EN 10216-2: 2014 Seamless steel tubes for pressure purposes. Technical delivery conditions. Non-alloy and alloy steel tubes with specified elevated temperature properties

[13] ∗ ∗ ∗ EN 10253 – 3:2008 Butt-welding pipe fittings Part 3: Wrought austenitic and austenitic-ferritic (duplex) stainless steels without specific inspection requirements

[14] ∗ ∗ ∗ EN 13480 – 3:2012 Metallic industrial piping – Part 3: Design and calculation